

JGR Biogeosciences

RESEARCH ARTICLE

10.1029/2019JG005620

Key Points:

- Long-term pH and Ω_{Ar} increases in the upper bay were consistent with increased alkalization of the Susquehanna River
- Long-term midbay pH variability was influenced by OA and biological processes, while Ω_{Ar} was generally regulated by OA and river basification
- Significant long-term pH and Ω_{Ar} declines in the lower bay were driven by nearly equal contributions from OA and net ecosystem production

Supporting Information:

- Supporting Information S1

Correspondence to:

C. Shen,
cshen@umces.edu

Citation:

Shen, C., Testa, J. M., Li, M., & Cai, W.-J. (2020). Understanding anthropogenic impacts on pH and aragonite saturation state in Chesapeake Bay: Insights from a 30-year model study. *Journal of Geophysical Research: Biogeosciences*, 125, e2019JG005620. <https://doi.org/10.1029/2019JG005620>

Received 21 DEC 2019

Accepted 18 MAY 2020

Accepted article online 29 MAY 2020

Understanding Anthropogenic Impacts on pH and Aragonite Saturation State in Chesapeake Bay: Insights From a 30-Year Model Study

Chunqi Shen¹ , Jeremy M. Testa¹ , Ming Li² , and Wei-Jun Cai³ 

¹Chesapeake Biological Laboratory, University of Maryland Center for Environmental Science, Solomons, MD, USA,

²Horn Point Laboratory, University of Maryland Center for Environmental Science, Cambridge, MD, USA, ³School of Marine Science and Policy, University of Delaware, Newark, DE, USA

Abstract Ocean acidification (OA) is often defined as the gradual decline in pH and aragonite saturation state (Ω_{Ar}) for open ocean waters as a result of increasing atmospheric pCO_2 . Potential long-term trends in pH and Ω_{Ar} in estuarine environments are often obscured by a variety of other factors, including changes in watershed land use and associated riverine carbonate chemistry and estuarine ecosystem metabolism. In this work, we investigated the anthropogenic impacts on pH and Ω_{Ar} over three decades (1986–2015) in Chesapeake Bay using retrospective coupled hydrodynamic-biogeochemical model simulations. Simulation results demonstrated a clear estuarine acidification signal in the midbay region, with a long-term increase in the annual duration of acidified bottom waters (pH < 7.5, ~2 days/yr) as well as a shallowing of the saturation horizon (~0.1 m/yr). In contrast, scenario results revealed basification in the upper bay consistent with increased alkalization of the Susquehanna River. Significant long-term pH and Ω_{Ar} declines in the lower bay were driven by nearly equal contributions from OA and lowered surface ecosystem production. The midbay pH variability was primarily influenced by OA and biological processes, while river basification along with OA played a key role in regulating the long-term Ω_{Ar} variability. This study quantifies the contributions from multiple anthropogenic drivers to changes in estuarine carbonate chemistry over three decades, highlighting the complex interactions in regulating the dynamics of pH and Ω_{Ar} and informing regional natural resource management and ecosystem restoration.

1. Introduction

Ocean acidification (OA) is often defined as the gradual decline in pH (~0.11 since the industrial revolution) and saturation state of calcium carbonate minerals (Ω_{Ar} , ~0.5 with respect to aragonite) for surface open-ocean waters as a result of increasing atmospheric pCO_2 (Feely et al., 2004). In addition to the well-studied trends in the open ocean, variability of pH and saturation state at shorter time scales in coastal areas has been explored through field observations and modeling approaches in the Gulf of Mexico (Cai et al., 2011; Laurent et al., 2017, 2018; Sunda & Cai, 2012), Baltic Sea (Carstensen et al., 2018; Müller et al., 2016), East China Sea (Cai et al., 2011), California Current (Feely et al., 2018; Hauri et al., 2013), and Gulf of Alaska (Pilcher et al., 2019; Siedlecki et al., 2017). These studies have displayed high spatial and temporal variability and complex controls on coastal pH and saturation state resulting from the interplay of exchanges with the open ocean and atmosphere, watershed inputs, and intense ecosystem metabolism in both deep and shallow water habitats (Bauer et al., 2013; Regnier et al., 2013). These complexities present a challenge for managing and anticipating acidification effects in coastal environments, which are critical natural habitats for many ecologically and economically important organisms (Waldbusser & Salisbury, 2014).

Previous efforts to understand long-term drivers of pH have revealed that the pH decline in coastal environments can be much larger than that predicted from ocean acidification (Cai et al., 2011; Duarte et al., 2013; Feely et al., 2010; Van Dam & Wang, 2019; Waldbusser et al., 2011) and that increasingly acidified water may place significant impacts on marine calcifiers (Long et al., 2016; Waldbusser et al., 2015). In contrast, changes in land use and increasing runoff can enhance alkalinity export from land to coastal ecosystems through chemical weathering (Raymond et al., 2008). For example, human-accelerated weathering has been linked to statistically significant increasing trends in alkalinity in the eastern United States, where increased

river alkalization was observed at over 60% of total 97 sites (Kaushal et al., 2013). Similarly, increasing pH trends were typical in freshwater rivers and streams throughout all regions of the contiguous United States (Kaushal et al., 2018). The enhanced buffering associated with elevated alkalinity and pH in riverine waters (i.e., river basification) may counteract the tendency for pH and Ω_{Ar} to decline in coastal waters as a result of ocean acidification due to anthropogenic CO₂ emissions. Furthermore, human activities continue to alter watershed exports of nutrients and particulate organic matter, which control rates of estuarine and coastal ecosystem metabolism (Herrmann et al., 2015; Kemp et al., 1997) and therefore regulate carbonate chemistry in coastal environments. For example, long-term pH declines were absent or muted in shallow estuarine systems receiving large riverine nutrient inputs due to high CO₂ uptake through enhanced primary production (Borges & Gypens, 2010). Conversely, oxidation of organic matter originating from eutrophic surface layers can produce high CO₂ levels in the subsurface waters during summer, leading to rapid pH declines (Cai et al., 2011; Hagens et al., 2015; Mucci et al., 2011; Wallace et al., 2014).

Chesapeake Bay was once a habitat with abundant commercially important shell forming organisms and also suffers from chronic eutrophication, where elevated inputs of nutrients and organic matter have fueled the development of estuarine hypoxia (Hagy et al., 2004; Testa & Kemp, 2012) and acidification (Shen et al., 2019). Bay-wide watershed management of nutrient inputs aimed at limiting eutrophication and hypoxia may also influence spatiotemporal variability of pH and saturation state by regulating internal metabolic processes (e.g., respiratory CO₂ production). Analyses of 24 years (1985–2008) of observations revealed statistically significant declines in seasonally averaged daytime pH within polyhaline surface waters, but found a general increasing pH trend in oligohaline and mesohaline waters (the upper parts of the estuary) during summer (Waldbusser et al., 2011). Long-term observations within the major freshwater sources to Chesapeake Bay revealed robust basification signals, particularly in the Susquehanna River which contributes over half of the freshwater to the main stem (Kaushal et al., 2013, 2018). While this river “basification” could possibly increase the pH and saturation state in the very upper bay through direct inputs of highly buffered water, the long-term variability of carbonate chemistry along the full salinity gradient from freshwater to ocean waters (particularly for the middle and lower bay) is less clear.

Existing experimental work and field observations are inadequate to isolate and quantify the contributions of multiple anthropogenic controls on pH and saturation state in coastal environments, due to complex physical-biogeochemical interactions and limited spatiotemporal coverage in observations. In this study, we overcame these limitations by implementing a high-resolution, regional hydrodynamic-biogeochemical model that explicitly accounts for variable anthropogenic drivers on carbonate chemistry over a period constrained by observations. The model was configured for 30-year retrospective simulations (1986–2015) where the effects of three anthropogenic signals were removed to identify and quantify the key processes (including ocean acidification, tributary basification, and estuarine metabolism) in affecting bay-wide long-term variability of pH and Ω_{Ar} over regional and seasonal scales. Our findings highlight the seasonal dependence of regional trends in pH and Ω_{Ar} to specific external drivers, which can be used to inform regional watershed management and investigations of other large eutrophic environments under pressure of significant anthropogenic perturbations.

2. Materials and Methods

The hydrodynamic model used in this study is the Regional Ocean Modeling System (ROMS) configured for Chesapeake Bay as described by Li et al. (2005) and Zhong and Li (2006). The domain extends from the Susquehanna River to the Mid-Atlantic Bight with a mesh grid of 80 × 120 cells (~1-km width, Figure 1). The model adopts the sigma coordinate system in the vertical direction and is set up with 20 layers uniformly. The biogeochemical model Row Column Aesop (RCA) simulates two phytoplankton groups, as well as state variables representing particulate and dissolved organic carbon, nitrogen and phosphorus, dissolved inorganic nitrogen, phosphorus, silica, and O₂ (Li et al., 2016; Testa et al., 2014). It also includes a two-layer sediment diagenesis module which simulates the cycling of carbon, nitrogen, phosphorus, silica, sulfur, and O₂ (Brady et al., 2013; Testa et al., 2013). Hourly averages of physical outputs from ROMS were used to calculate the advection and diffusion of state variables in RCA. Riverine nutrient and organic matter inputs were obtained from routine monitoring stations in eight major river tributaries of the bay. We did not include direct inputs of organic matter and nutrients to tidal waters from atmospheric deposition and

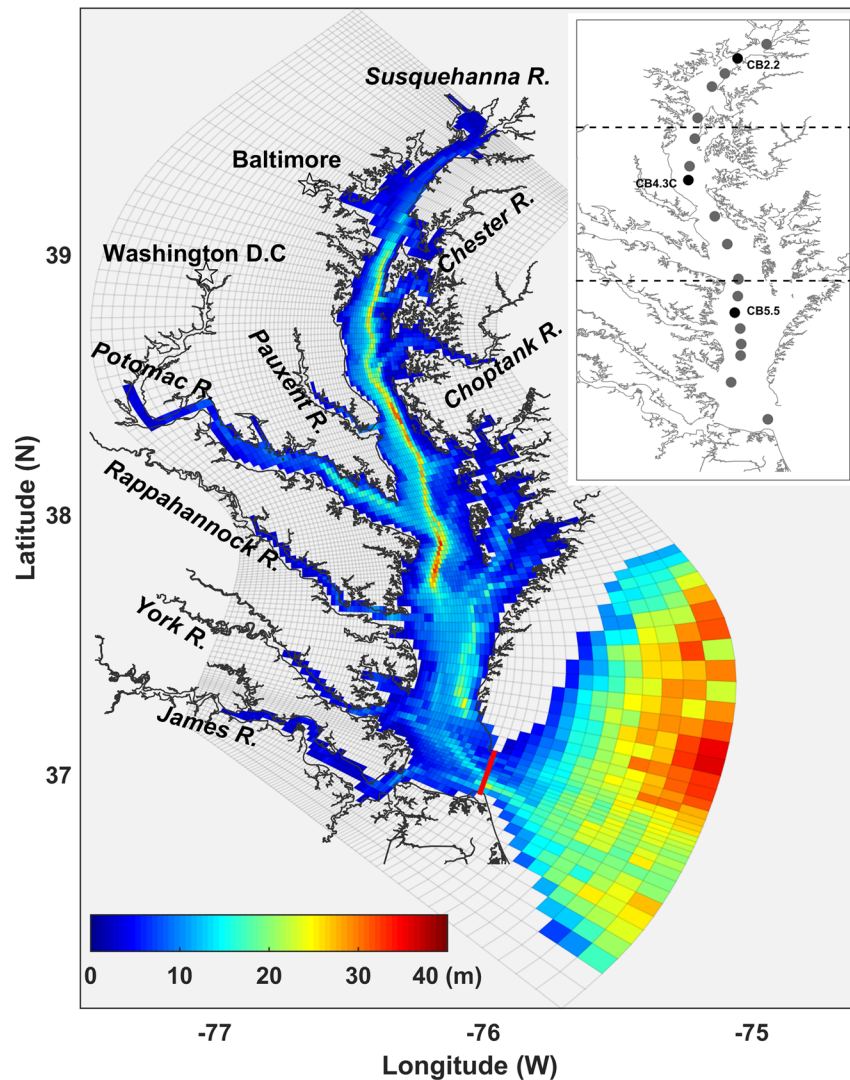


Figure 1. Bathymetry, tributaries, and the model grid of Chesapeake Bay. The inset figure displays routine, long-term monitoring stations along the main stem of the estuary. The dashed lines represent the boundaries between upper, mid, and lower bay.

point source loading given that the majority of these input changes are captured in fall line inputs. A detailed description of the model configuration was presented in Testa et al. (2014).

A carbonate chemistry module is coupled to RCA and tracks carbonate chemistry variables including dissolved inorganic carbon (DIC), total alkalinity (TA), and aragonite CaCO_3 . The module has been previously validated against a diversity of field observations (rate processes, concentrations) measured in 2016, and successfully reproduced vertical and horizontal gradients of pH, DIC, and TA over an annual cycle (Shen et al., 2019). The most important internal sources (and sinks) for the water column carbonate state variables (DIC, TA, CaCO_3) in the model include primary production/respiration, nitrification/denitrification, sulfate reduction and oxidation, calcium carbonate precipitation/dissolution, and sediment-water exchange. Air sea flux is parameterized as a function of transfer velocity, solubility, and the $p\text{CO}_2$ difference between surface water and the overlying atmosphere and only affects the DIC in the model. Other components of the carbonate chemistry system including pH (NBS scale), CO_2 , HCO_3^- , CO_3^{2-} , $p\text{CO}_2$, and Ω_{Ar} are diagnostically calculated based on the model outputs (e.g., salinity, temperature, DIC, TA, silica, and phosphate) with the CO2SYS program (Lewis & Wallace, 1998). For the calculations, the dissociation constants (K1 and K2) were used following Cai and Wang (1998), and KHSO_4 was from Dickson et al. (1990). Ω_{Ar} is computed as a

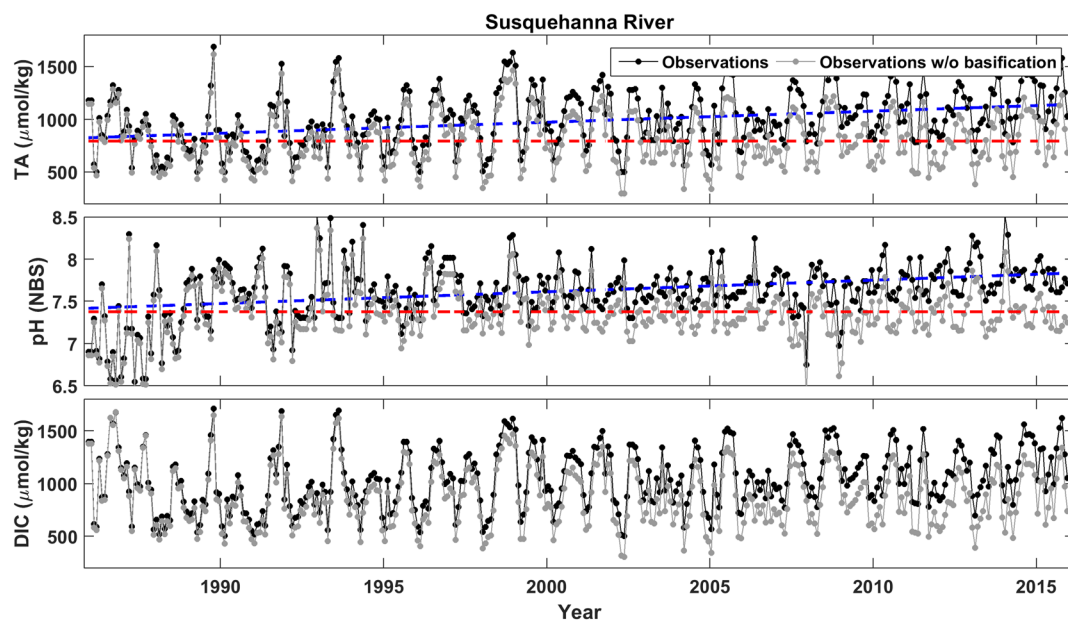


Figure 2. Time series of carbonate system properties in the Susquehanna River from 1986–2015, including the observed values (black circles) and values detrended to remove the long-term increases in TA and pH (gray circles). (upper panel) Total alkalinity, (middle panel) pH, and (lower panel) calculated DIC with alkalinity and pH. The dashed lines are the best fit for the long-term trends in these two data sets.

function (Equation 1) of the concentrations of calcium ion (Ca^{2+}) and CO_3^{2-} , as well as the temperature and pressure-dependent stoichiometric solubility product with respect to aragonite (K_{sp}).

$$\Omega_{\text{Ar}} = [\text{Ca}^{2+}] [\text{CO}_3^{2-}] / K_{\text{sp}} \quad (1)$$

While previous modeling efforts in Chesapeake Bay addressed spatial and seasonal patterns in carbonate system processes and concentrations in a single year (Shen et al., 2019), here we sought to understand controls on long-term trends in carbonate system properties (e.g., Waldbusser et al., 2011). To disentangle the impacts of variable anthropogenic forcing on the long-term variability of pH and Ω_{Ar} in Chesapeake Bay, we designed three model sensitivity scenarios, which included a realistic retrospective simulation (from 1986–2015) forced by the observed riverine, atmospheric, and ocean boundary conditions (“Base” simulation), a scenario that omitted ocean acidification from the atmosphere and adjacent coastal ocean (NOA), and a scenario where river basification associated with long-term increases in riverine TA and pH was omitted (NBasi). The model was forced by riverine inputs from eight major tributaries to Chesapeake Bay, of which the Susquehanna and Potomac Rivers contribute 80% of the flow (see Table S1 in the supporting information). We altered the nutrient and carbonate chemistry trends in a subset of these rivers to accomplish model scenarios. For the Base simulation, TA at the freshwater boundary was prepared with long-term historical observational data at nearby USGS stations (Figure 2). DIC concentrations during the simulation period (1986–2015) were not measured, and river boundary DIC concentrations were calculated through CO2SYS with the available TA and pH measurements. While the historical pH data, typically measured using glass electrodes, tends to have a relatively high uncertainty, we performed a comparison (Figure S1) between the calculated DIC (from pH and TA in measured in 2016) and observed DIC at station CB1.1 (mean salinity = 0.1). The calculated DIC was extremely close to DIC measured in 2016, with ~1% relative absolute error, suggesting that our calculated long-term DIC can accurately represent the freshwater boundary forcing. We also recomputed the pH time series of the Susquehanna River 200 times assuming the potential for all pH observations to vary within a range of 0.1 pH units. The results suggest a maximum potential change in the pH slope of ~9% (Figure S2), which is not large enough to likely overcome the reported trends. Ca^{2+} for the Ω_{Ar} calculation was not dynamically simulated in the model and was approximated using a linear regression to salinity instead (Riley & Tongudai, 1967). As this approximation

approaches zero at the freshwater endmember, which significantly underestimates the freshwater saturation state, we used observed Ca^{2+} concentrations (USGS) at regions where salinity <1.0 psu. At salinity >1.0 psu, the difference is small as the oceanic Ca^{2+} component increases rapidly. TA at the ocean boundary for the Base run was calculated through the empirical linear relationship ($\text{TA} = 47.59 \cdot \text{Sal} + 640.77$, $r^2 = 95\%$) fitted with cruise data from East Coast Program (Brodeur et al., 2019). Ocean boundary DIC was calculated with the available TA, $f\text{CO}_2$ from SOCAT (Bakker et al., 2016), salinity, and temperature using CO2SYS. Atmospheric $p\text{CO}_2$ data were obtained from NOAA-ESRL (<https://www.esrl.noaa.gov/gmd/ccgg/trends/>) with ~ 1.8 ppm increase each year.

The major tributaries of Chesapeake Bay were characterized by significant increases of TA and pH over the past several decades, with particularly strong increases in the Susquehanna River that had an average increase rate of $12 \mu\text{mol kg}^{-1}$ per year for TA and 0.015 units per year for pH, respectively, from 1986 to 2015 (Figure 2). We detrended the TA and pH in riverine inputs over the simulation period to generate inputs without long-term basification (Figures 2 and S3–S5). The NBasi scenario was therefore driven by the new tributary inputs (e.g., TA, DIC) while the other forcing from the Base scenario was kept the same. Historical TA data at the lower bay area (Rappahannock River, James River, and York River) were not available and were derived through TA-discharge relationship based on limited field measurements. We used the same TA and pH data for these lower bay rivers in the Base and NBasi scenarios. While this study focused on external changes in carbonate system forcing, we also note that nitrate + nitrite ($\text{NO}_3^- + \text{NO}_2^-$) loading from the Susquehanna River decreased $\sim 14\%$ (Figure S6) over the timeframe of our simulations (e.g., Zhang et al., 2015). Thus, we also performed a simulation where the long-term nitrate and nitrite reduction from the Susquehanna River was removed to simulate the potential impact of nutrient reductions on the modeled pH trends. The scenario run without ocean acidification (NOA) used the same driving forcing as the Base run, except the ocean TA/DIC boundary and the atmospheric $p\text{CO}_2$ levels, which were all forced to the same level as those of year 1986 (first year of simulations), assuming no impacts from anthropogenic CO_2 emissions over the past 30 years.

The coupled hydrodynamic-biogeochemical model has been validated against a wide range of observed biogeochemical rate and concentration data (e.g., Chl *a*, ammonium, particulate organic carbon, DIC, TA, primary production/respiration, sediment-water fluxes) in Chesapeake Bay at multiple time and space scales (Li et al., 2016; Shen et al., 2019; Testa et al., 2014; Zhong & Li, 2006). Field observations (since 1984) along the main stem (Figure 1) were collected by the Chesapeake Bay Program and can be accessed through the data portal (<http://data.chesapeakebay.net>). In this study, we compared the long-term pH trends in the upper, mid, and lower bay between the model simulations and observations. Analyses of long-term pH and Ω_{Ar} variability between different scenarios focused on the spring and summer periods. The spring includes months of April, May, and June, and summer includes June, July, August, and September, corresponding to important growth periods for adult and juvenile oysters, respectively (Waldbusser et al., 2011). The average spring discharge of Susquehanna River over 1986–2015 was roughly $1,400 \text{ m}^3 \text{ s}^{-1}$, compared to $600 \text{ m}^3 \text{ s}^{-1}$ in summer.

3. Results and Discussion

3.1. Patterns of pH and Ω_{Ar} in Chesapeake Bay

We compared simulation results with historical observations of pH along the main stem of Chesapeake Bay, where the model favorably predicted the surface (RMSE = 0.27, $r = 0.73$, $p < 0.001$) and bottom (RMSE = 0.22, $r = 0.72$, $p < 0.001$) pH in the upper (CB2.2, mean salinity = 2.3), middle (CB4.3C, mean salinity = 12.2), and lower bay (CB5.5, mean salinity = 16.5), respectively (Figure 3). The RMSE of pH comparisons, if averaged over spring and summer, reduced to 0.18 for surface waters and 0.14 for bottom waters. Both field observations and model predictions displayed greater pH variability of surface waters along the main channel relative to bottom waters, reflecting that surface water carbonate chemistry was regulated by multiple physical and biogeochemical processes (e.g., photosynthesis, respiration, air-sea exchange, freshwater-ocean water mixing). pH was lower in the upper bay (mean pH = 7.6) than seaward regions (mean pH = 8.1) throughout the water column, as it was more directly influenced by the freshwater discharge with comparably lower pH and buffer capacity. Summer pH variations within midbay surface and bottom waters were particularly strong as a result of seasonal stratification (e.g., Murphy et al., 2011) and

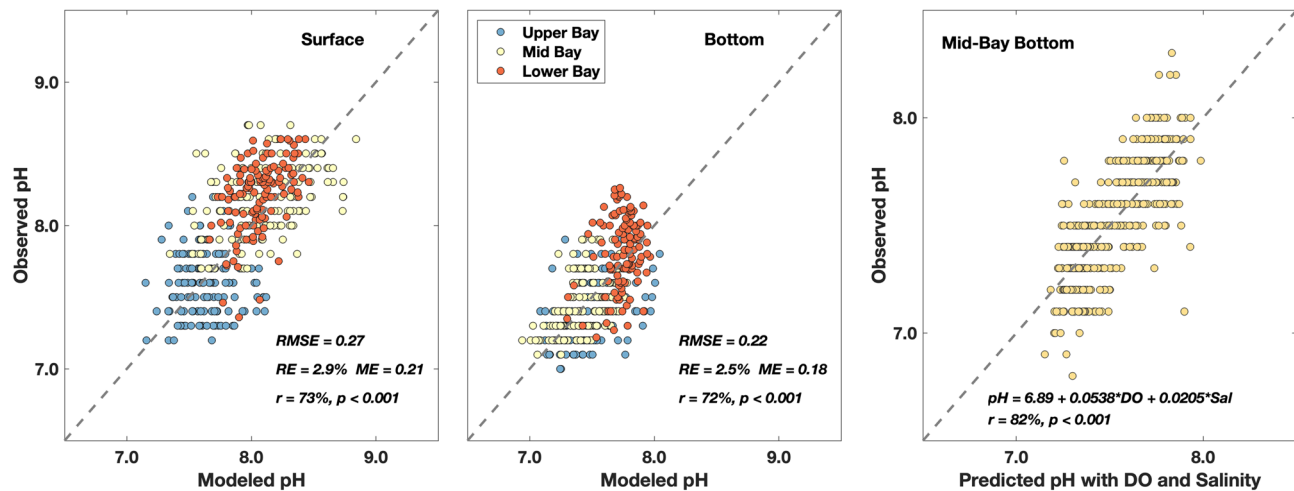


Figure 3. Comparisons of pH between observations and simulations at stations in the upper (CB2.2), middle (CB4.3), and lower (CB5.5) Chesapeake Bay including surface waters (left panel), bottom waters (middle panel), and observed pH in the mid-bay bottom versus pH predicted from dissolved oxygen and salinity (right panel). RMSE represents root-mean-square error, RE represents relative absolute error, ME is the mean absolute error, and r is the correlation coefficient.

the subsequent decoupling of surface photosynthesis and bottom respiration (Shen et al., 2019). Consequently, midbay bottom waters were vulnerable to hypoxia and acidification, with extremely low DO and pH during summer (Cai et al., 2017; Li et al., 2016). DO was a highly significant predictor of pH, especially in hypoxic regions where respiration is the dominant process regulating pH and DO via CO_2 production and O_2 consumption (Feely et al., 2018; Shen et al., 2019). Salinity was also an important covariate with pH in the midbay bottom, as revealed from a multiple linear regression model (Figure 3) that explained a large fraction of observed pH variability from DO and salinity ($r = 0.82$, $p < 0.001$). Here, the DO variation reflects respiration effects on pH (via CO_2 production), while salinity reveals the impacts of wet/dry season alternations in freshwater influence and seasonal variations of buffer capacity associated with the encroachment of higher TA/higher salinity oceanic water during the low-flow summer period. The remaining unexplained variability reveals potential contributions from calcium carbonate dissolution (Cai et al., 2017), nitrification/denitrification (Testa et al., 2018), and sulfate reduction (Marvin-DiPasquale & Capone, 1998) that are regionally and seasonally important. In a large region of bottom water in the middle and lower bay, where $\text{DO} = 0$ and salinity is ~ 20 , pH approaches 7.3. This is a state of pH controlled jointly by complete aerobic oxygen consumption (bringing pH to 7.2) and modified by sulfate reduction and the existence of H_2S (bringing pH to slightly below 7.2), and CaCO_3 dissolution that buffers against pH declines (Cai et al., 2017).

The long-term averaged, modeled vertical profile of Ω_{Ar} along the main stem displayed large temporal and spatial variations (Figure 4), revealing seasonally varying controls along the salinity gradient. In general, Ω_{Ar} increased with salinity in the along-channel direction and decreased with depth, which was consistent with the patterns and values derived from field measurements in 2016 (Brodeur et al., 2019) and with the spatial distribution of pH presented in previous studies (Shen et al., 2019). The upper bay was undersaturated ($\Omega_{\text{Ar}} < 1$; with 98.5% and 93.4% of the total volume in spring and summer) across the entire water column, primarily due to the low Ca^{2+} concentrations, although observed Ca^{2+} data in low salinity regions were used for calculation to avoid underestimations (see section 2). The lower bay was typically supersaturated ($\Omega_{\text{Ar}} > 1$) during spring (82.3%) and summer (97.2%) through mixing with the coastal ocean where Ω_{Ar} is ~ 2.5 (Xu et al., 2017). Ω_{Ar} in the mid bay varied considerably through the water-column, with oversaturation (mean $\Omega_{\text{Ar}} = 1.45$) in the surface waters and undersaturation (mean $\Omega_{\text{Ar}} = 0.72$) in the bottom waters. This was particularly clear during the summer months (surface $\Omega_{\text{Ar}} = 1.86$, bottom $\Omega_{\text{Ar}} = 0.84$) when stable stratification developed, allowing for net CO_2 uptake in productive surface waters and net CO_2 production in respiration-dominated bottom waters (e.g., Kemp et al., 1997; Smith & Kemp, 1995). Model results revealed that Ω_{Ar} was higher in summer than in spring, as summer is typified by comparably lower riverine runoff from

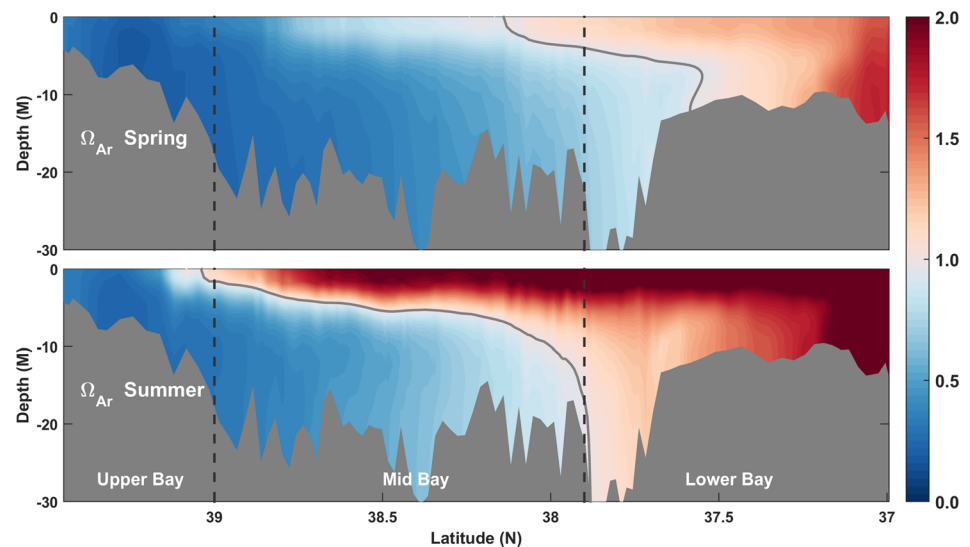


Figure 4. Along-channel distribution of long-term averaged aragonite saturation state (Ω_{Ar}) during spring (upper panel) and summer (lower panel). The gray line represents the saturation horizon of $\Omega_{Ar} = 1.0$.

tributaries (e.g., Brodeur et al., 2019). A second consequence of low flow during summer is the northward migration of the aragonite saturation horizon ($\Omega_{Ar} = 1.0$) toward the low-salinity region (Figure 4), thereby reducing the undersaturation (dissolution favorable) volume for the main stem of Chesapeake Bay. In fact, undersaturated water occupied over half of the main stem in spring with an average ratio of 55%, while this ratio declined to nearly 28% during summer period according to the simulations.

3.2. pH and Ω_{Ar} Trends During 1986–2015

We examined the low-pH duration (i.e., number of days per year when $\text{pH} < 7.5$) across the bottom of Chesapeake Bay for the 30-year simulation. Spatial variability along the salinity gradient was evident (Figure 5), where bottom water in the lower bay and its tributaries, which frequently exchanged with Mid-Atlantic Bight water, was characterized by pH typically >8.0 . As such, no significant change in low-pH duration was observed in the lower bay over the past 30 years. Simulations illustrated substantial low-pH bottom water within the upper and midbay, where the mean annual duration reached its maximum (~ 200 days) within the upper to middle bay transition region (Figure 5a), consistent with relatively lower buffer capacity and high respiration rates (e.g., Cai et al., 2017; Smith & Kemp, 1995). A long-term increasing trend of 1.0 day yr^{-1} was observed at the bottom of this transition zone (Figure 5b), indicating gradual acidification over the past 30 years, but in the central, seaward midbay bottom waters, the longest annual duration increases occurred with an average trend of 2 days yr^{-1} (i.e., ~ 2 -month increase from 1986 to 2015). In contrast, the very upper bay where salinity is typically <5.0 displayed the opposite trend, including a shorter duration at its bottom, possibly resulting from increased alkalinity and pH of freshwater inputs from the Susquehanna River (Figure 2; Kaushal et al., 2013), increased Chl *a* (Testa et al., 2018; and presumably primary production), or both.

We also estimated the position of the aragonite saturation horizon ($\Omega_{Ar} = 1.0$) relative to the depth of the water column across the main stem over the past three decades. This horizon in the midbay displayed a relatively complex pattern, with oversaturation in the shallow flanks and surface waters of the deep central channel (Figure 6a, 100% represents the entire column is saturated), but undersaturation in the bottom waters of the deep central channel (0% represents that the entire column is undersaturated). This is consistent with the pattern of ecosystem metabolism in the midbay and other estuarine systems, with net autotrophy (primary production greater than total respiration) in the shallow nearshore area, but net heterotrophy in the deep central channel where pH and Ω_{Ar} are consistently low (Crosswell et al., 2017; Testa et al., 2014). No significant long-term trends were noted in low salinity regions, where model results suggested that the shallow upper bay was consistently undersaturated due to influence by freshwater inputs and high

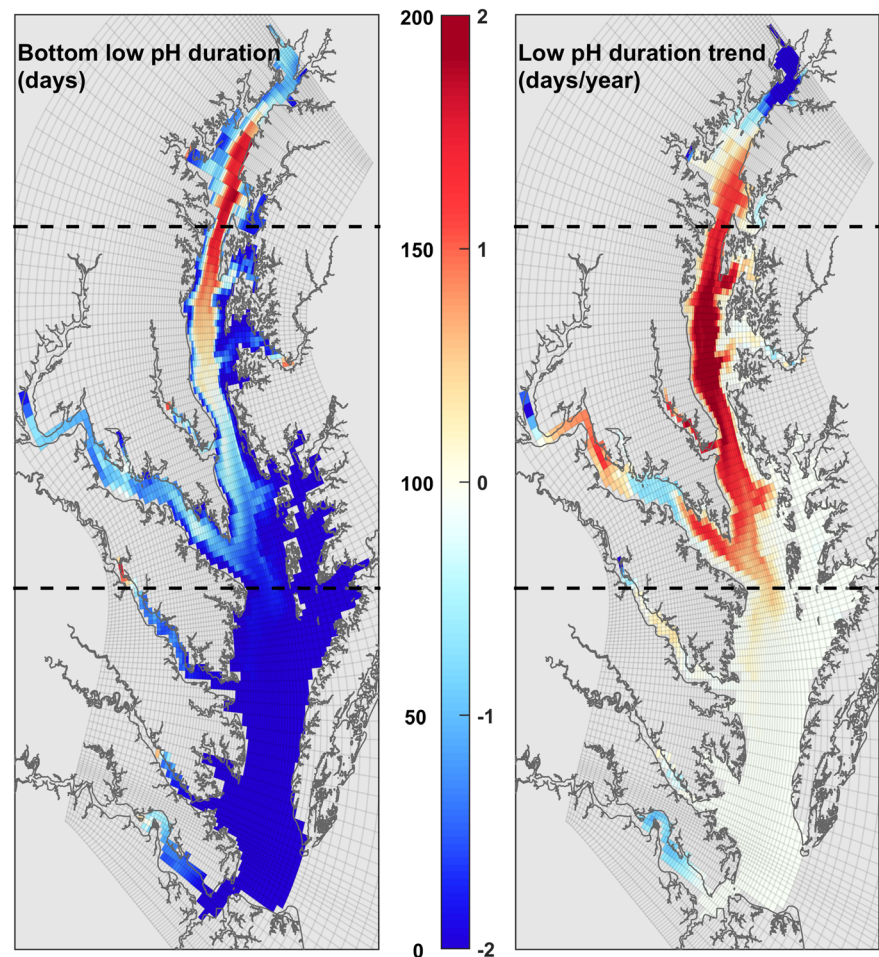


Figure 5. (left panel) Model-simulated mean annual low-pH duration (days of $\text{pH} < 7.5$) in the bottom waters of Chesapeake Bay during 1986–2015. (right panel) Long-term trends (days per year) of the low-pH duration from 1986–2015 in the bottom of Chesapeake Bay. Negative trends (e.g., the upper bay) represent a decreasing annual low-pH duration while positive trends (e.g., the midbay) represent an increasing annual low-pH duration.

rates of respiration and associated CO_2 production (Kemp et al., 1997). In contrast, the high salinity lower bay region was consistently supersaturated without obvious long-term trends in the aragonite saturation horizon. Modeled Ω_{Ar} in the central midbay displayed a shoaling saturation horizon over the years (i.e., low Ω_{Ar} at increasingly shallow depths, Figure 6b), where the lower reach of midbay had a shoaling rate of 0.2 m/year (6.0 m from 1986 to 2015). Over the entire main stem, the model indicated an increasing long-term undersaturation volume ($\sim 0.3\%$ expansion per year).

We compared the long-term modeled trends of surface water pH with observations along the central main stem to allow for a model diagnosis of controls on long-term changes. Modeled 30-year pH trends were consistent with observations in the upper and lower bay (Figure 7, Table 1). While the model slightly underestimated the observed seasonally (spring and summer) averaged pH and its trend in the lower bay region, trends from both data sets revealed statistically significant declines in pH from 1986–2015 (the spring season had an even stronger pH decline), consistent with prior analyses (Waldbusser et al., 2011). Modeled long-term pH trends in the upper bay were also consistent with observations, where in contrast to the lower bay, the upper bay trend was positive (an overall pH increase) over the past three decades. In both the upper and lower bay, despite opposing directions of pH change, both the observational data and simulations demonstrated stronger (increasing/decreasing) trends in spring than during summer. Discrepancies between observations and simulations were evident in the midbay region during spring, where

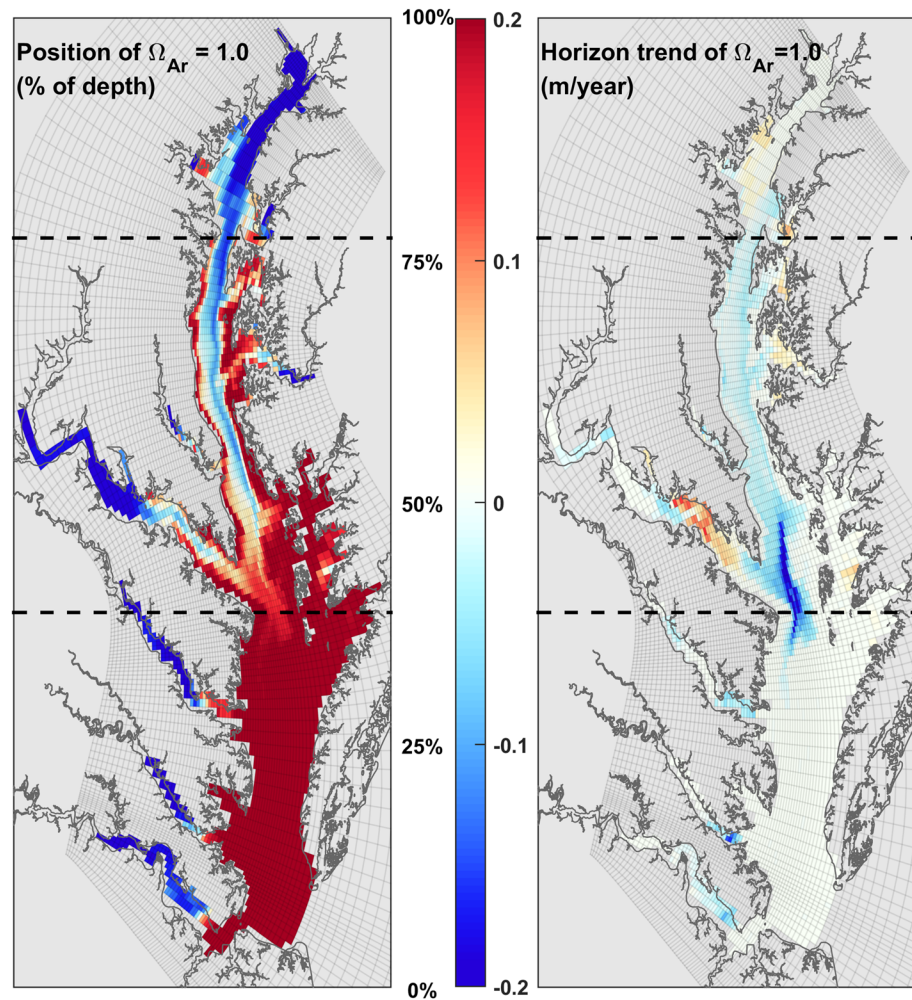


Figure 6. (left panel) Mean annual positions (relative to the depth) of the aragonite saturation horizon during 1986–2015. 100% means the entire water column is saturated with respect to aragonite whereas 0% means the entire water depth is undersaturated. (right panel) Long-term trends (m/year) of the saturation horizon position. Negative trends represent a shallowing saturation horizon depth (or an increasing undersaturated volume).

observational data showed an increasing trend similar to the upper bay, and model simulations indicated a long-term pH decline. The midbay serves as a transition between waters highly influenced by freshwater inputs (where alkalinity has increased) and those that exchange substantially with the coastal ocean (where acidification has occurred), and is a region where primary production and respiration rates are typically highest bay-wide (Kemp et al., 1997; Smith & Kemp, 1995). Long-term surface simulated and observed Chl *a* concentration trends also differed during spring in this region, where observations suggested a long-term increase (consistent with a pH increase) and model simulations showed no trend (Figure S7). This model-observation discrepancy suggests that the pH discrepancies in the midbay during spring could possibly result from the bias in surface primary production and/or phytoplankton biomass. The long-term trends of surface water Ω_{Ar} along the main channel followed the patterns of simulated surface pH (Figure 9, Table 2), with significant and moderate declines in the lower and midbay, respectively, but an increase in the upper bay.

3.3. Anthropogenic Impacts to the Main-Stem Surface Waters

To discern the role of external versus internal controls on long-term pH and Ω_{Ar} trends, we compared realistic hindcast simulations (“Base”) with idealized hindcasts that removed trends in atmospheric plus coastal ocean acidification (NOA). Comparisons between results of Base and no ocean acidification scenarios

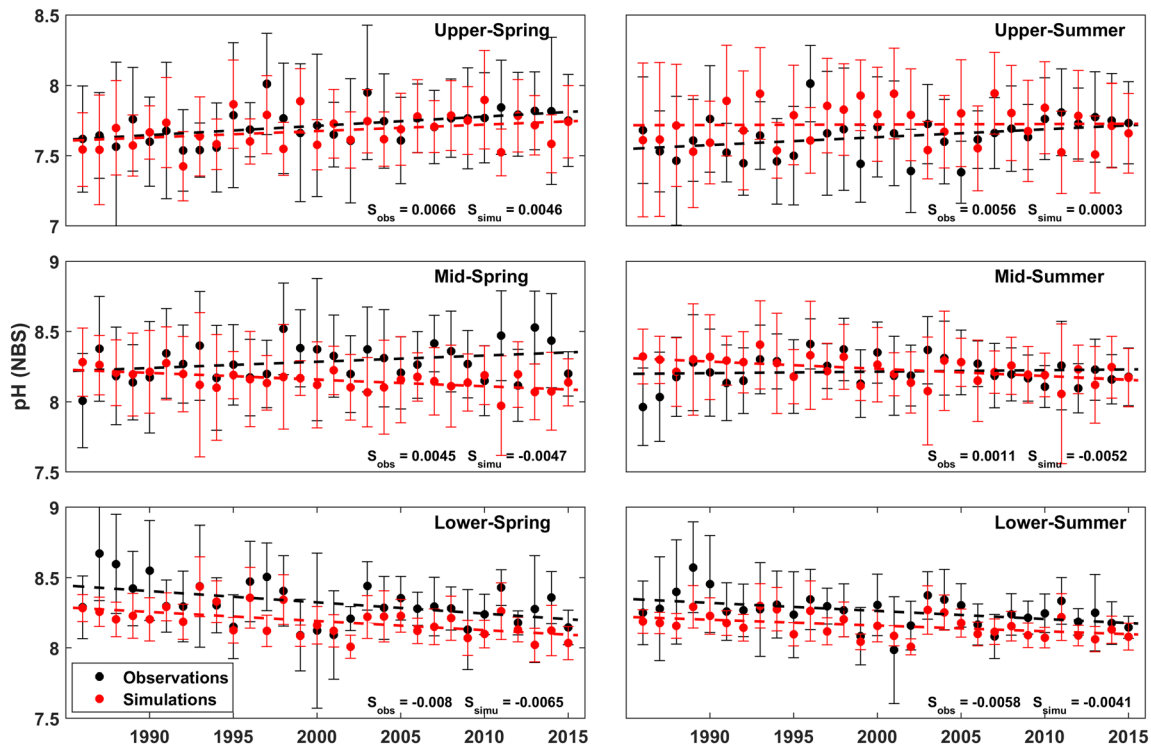


Figure 7. Comparisons of surface water pH between observations (black circles) and simulations (red circles) in spring and summer along the main stem. Error bars represent 1 standard deviation. The dashed lines represent best linear fit. Symbol S represents slope of the observed values (S_{obs}) and simulated values (S_{simu}).

Table 1
Trend Analyses for Surface Water pH in Spring and Summer Along the Main Stem

pH trend over 30 years		Fitted relationships pH = a*(#year) + b		Skill assessment	Δ pH/yr (Δ pH/30 yr)
Spring	Upper	Observations	$Y = 0.0066 * X + 7.6138$	$r = 0.51, p = 0.004$	0.0066(0.198)
		Model Base	$Y = 0.0050 * X + 7.5011$	$r = 0.37, p = 0.047$	0.0050(0.150)
		NOA	$Y = 0.0064 * X + 7.5008$	$r = 0.44, p = 0.016$	0.0064(0.192)
		NBasi	$Y = 0.0000 * X + 7.4764$	$r = 0.001, p = 0.99$	0.0000(0.000)
	Mid	Observations	$Y = 0.0045 * X + 8.2169$	$r = 0.31, p = 0.09$	0.0045(0.135)
		Model Base	$Y = -0.0043 * X + 8.1840$	$r = 0.58, p < 0.001$	-0.0043(-0.129)
		NOA	$Y = -0.0017 * X + 8.1846$	$r = 0.27, p = 0.14$	-0.0017(-0.051)
		NBasi	$Y = -0.0052 * X + 8.1827$	$r = 0.60, p < 0.001$	-0.0052(-0.156)
	Lower	Observations	$Y = -0.008 * X + 8.4439$	$r = 0.47, p = 0.009$	-0.0080(-0.240)
		Model Base	$Y = -0.0059 * X + 8.2300$	$r = 0.53, p = 0.002$	-0.0059(-0.177)
		NOA	$Y = -0.0035 * X + 8.2321$	$r = 0.33, p = 0.069$	-0.0035(-0.105)
		NBasi	$Y = -0.0063 * X + 8.2317$	$r = 0.55, p = 0.002$	-0.0063(-0.189)
Summer	Upper	Observations	$Y = 0.0056 * X + 7.5475$	$r = 0.35, p = 0.06$	0.0056(0.168)
		Model Base	$Y = 0.0011 * X + 7.6060$	$r = 0.07, p = 0.72$	0.0011(0.033)
		NOA	$Y = 0.0023 * X + 7.6062$	$r = 0.14, p = 0.46$	0.0023(0.069)
		NBasi	$Y = -0.0024 * X + 7.5956$	$r = 0.14, p = 0.46$	-0.0024(-0.072)
	Mid	Observations	$Y = 0.0011 * X + 8.1971$	$r = 0.09, p = 0.62$	0.0011(0.033)
		Model Base	$Y = -0.0047 * X + 8.2157$	$r = 0.58, p < 0.001$	-0.0047(-0.141)
		NOA	$Y = -0.0025 * X + 8.2151$	$r = 0.35, p = 0.058$	-0.0025(-0.075)
		NBasi	$Y = -0.0053 * X + 8.2190$	$r = 0.59, p < 0.001$	-0.0053(-0.159)
	Lower	Observations	$Y = -0.0058 * X + 8.3488$	$r = 0.44, p = 0.015$	-0.0058(-0.174)
		Model Base	$Y = -0.0038 * X + 8.1308$	$r = 0.47, p = 0.008$	-0.0038(-0.114)
		NOA	$Y = -0.0013 * X + 8.1302$	$r = 0.18, p = 0.34$	-0.0013(-0.039)
		NBasi	$Y = -0.0041 * X + 8.1320$	$r = 0.49, p = 0.005$	-0.0041(-0.123)

Note. Significant trends ($p < 0.05$) are highlighted in bold.

Table 2
Trend Analyses for Surface Water Ω_{Ar} During Spring and Summer Along the Main Stem

Ω_{Ar} trend over 30 years			Fitted relationships $pH = a*(\#year) + b$		Skill assessment	$\Delta \Omega/yr$ ($\Delta \Omega/30 yr$)
Spring	Upper	Model	Base	$Y = 0.0019*X + 0.28$	$r = 0.25, p = 0.18$	0.0019(0.057)
			NOA	$Y = 0.0026*X + 0.28$	$r = 0.32, p = 0.092$	0.0026(0.078)
			NBasi	$Y = 0.0004*X + 0.28$	$r = 0.07, p = 0.73$	0.0004(0.012)
	Mid	Model	Base	$Y = -0.002*X + 1.06$	$r = 0.11, p = 0.54$	-0.0020(-0.06)
			NOA	$Y = 0.003*X + 1.05$	$r = 0.15, p = 0.42$	0.0030(0.090)
			NBasi	$Y = -0.006*X + 1.05$	$r = 0.33, p = 0.07$	-0.0060(-0.180)
	Lower	Model	Base	$Y = -0.0094*X + 1.67$	$r = 0.68, p < 0.001$	-0.0094(-0.282)
			NOA	$Y = -0.003*X + 1.67$	$r = 0.26, p = 0.16$	-0.0030(-0.090)
			NBasi	$Y = -0.0122*X + 1.66$	$r = 0.79, p < 0.001$	-0.0122(-0.366)
Summer	Upper	Model	Base	$Y = 0.0012*X + 0.46$	$r = 0.08, p = 0.65$	0.0012(0.036)
			NOA	$Y = 0.0024*X + 0.46$	$r = 0.16, p = 0.41$	0.0024(0.072)
			NBasi	$Y = -0.0009*X + 0.46$	$r = 0.07, p = 0.72$	-0.0009(-0.027)
	Mid	Model	Base	$Y = -0.0032*X + 1.65$	$r = 0.18, p = 0.34$	-0.0032(-0.096)
			NOA	$Y = 0.0032*X + 1.66$	$r = 0.16, p = 0.38$	0.0032(0.096)
			NBasi	$Y = -0.0087*X + 1.64$	$r = 0.44, p = 0.01$	-0.0087(-0.261)
	Lower	Model	Base	$Y = -0.0074*X + 2.14$	$r = 0.54, p = 0.001$	-0.0074(-0.222)
			NOA	$Y = -0.0014*X + 2.14$	$r = 0.11, p = 0.56$	-0.0014(-0.042)
			NBasi	$Y = -0.0116*X + 2.13$	$r = 0.74, p < 0.001$	-0.0116(-0.348)

Note. Significant trends ($p < 0.05$) are highlighted in bold.

demonstrated that OA led to consistent declines of surface water pH and aragonite saturation in the upper, mid, and lower bay (Figures 8 and 9, Tables 1 and 2), even though the interannual variability was significant. Modeled OA effects on surface main stem waters did not indicate a seasonal dependence of OA variability; however, clear differences in vulnerability to OA were evident along the salinity gradient. Simulation results indicated a relatively weak OA signal in the upper bay with an average drop of 0.039 pH units over 1986–2015, while declines in the middle and lower bay were estimated as 0.072 and 0.074, respectively, due to

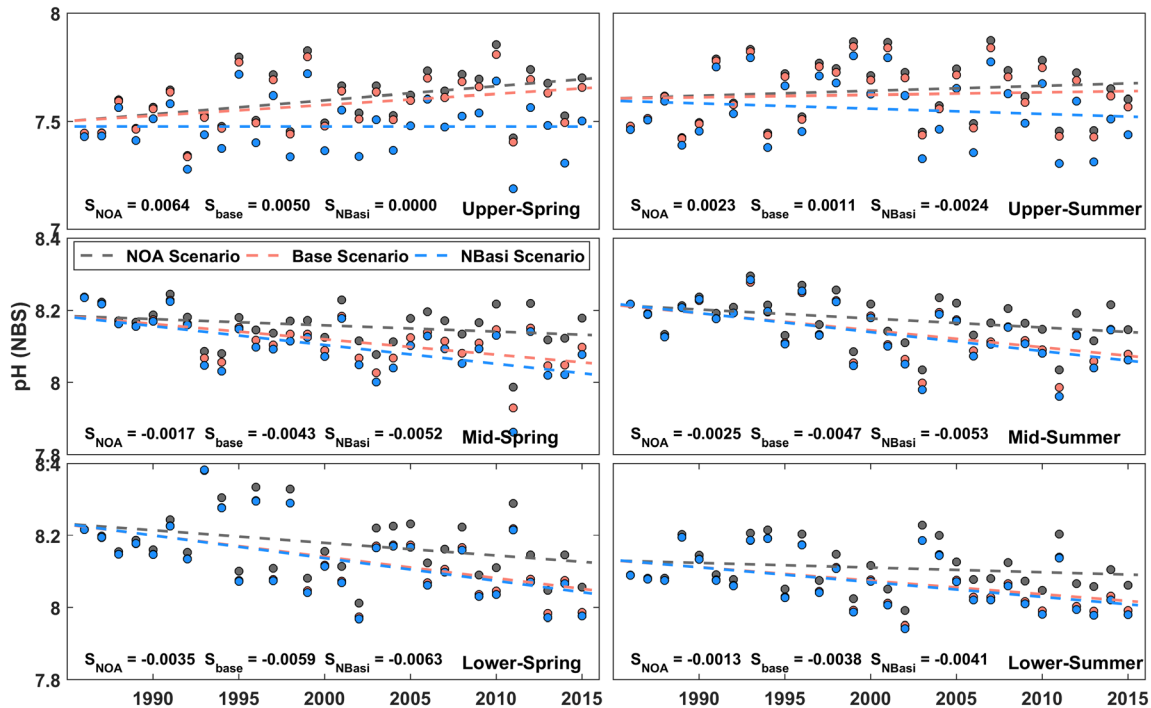


Figure 8. Comparisons of seasonally averaged surface water pH between different model scenarios (“base” simulation with all trends included, ocean acidification trend removed = “NOA,” and river basification removed = “NBasi”). The dashed lines represent best linear fit. Symbol S represents the slope of the best fit line for each scenario.

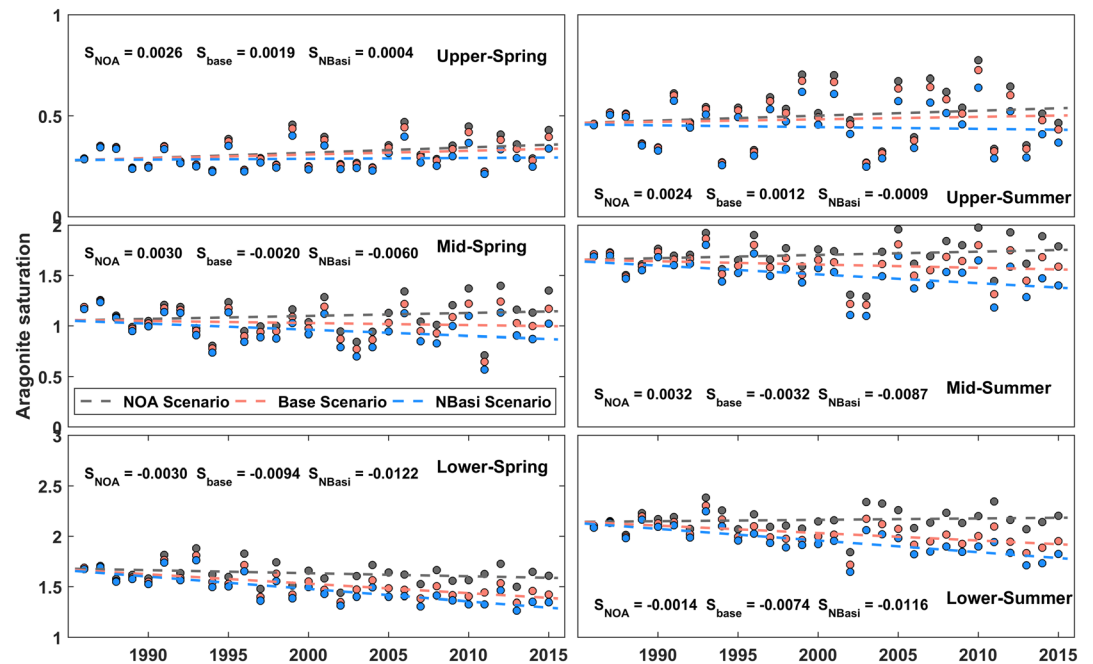


Figure 9. Comparisons of seasonally averaged surface water aragonite saturation state between different model scenarios (“base” simulation with all trends included, ocean acidification trend removed = “NOA,” and river basification removed = “NBasi”). The dashed lines represent best linear fit. Symbol S represents the slope of the best fit line for each scenario.

more substantial influence from acidifying coastal waters combined with the overall atmospheric $p\text{CO}_2$ increase (347 to 400 ppm from 1986–2015). Variability patterns of Ω_{Ar} were similar to those of pH under OA impacts. Ω_{Ar} of the Base scenario in the upper bay was slightly decreased (0.028 during 30-year simulation) compared to the NOA scenario. The long-term surface Ω_{Ar} decline due to OA in the midbay was 0.171, and the lower bay Ω_{Ar} decline reached 0.185.

In contrast to the OA effects, the scenario with the river basification trend removed (NBasi) showed that river basification buffered surface pH and Ω_{Ar} along the main stem (Figures 8 and 9, Tables 1 and 2). The pH increases due to river basification (TA or pH increase at the river endmember) in the upper bay were linked to direct inputs of Susquehanna River water. Seasonal variability resulting from basification was relatively larger than the OA effect due to wet/dry seasonal alternations, where the pH increase during the high flow spring period was 0.15, nearly 50% larger than the long-term increase during the low-flow summer period (-0.105). The middle and lower bay pH were less impacted by basification associated with Susquehanna River discharge, with little variability between the Base and NBasi scenarios. The long-term buffer effects on Ω_{Ar} due to river basification decreased as salinity increased (i.e., from the upper bay seaward to the lower bay), with an increase of 15.2%, 10.4%, and 5.5% in the upper, middle, and lower bay, respectively. Seasonally dependent changes in Ω_{Ar} were opposite to the effect of pH, with larger increases in summer when Ca^{2+} concentration was relatively higher along with lower river runoff and higher salinity.

The pH of open ocean surface waters decreased steadily over the last few decades at a rate of 0.0019 per year (0.057 for 30 years, Doney, 2010), and this trend generally matches expectations for OA driven by increasing atmospheric $p\text{CO}_2$. Our model results indicate a much stronger acidification signal in the lower bay (0.145 pH units) and a basification signal (0.12 pH units) in the upper bay, which suggests multiple processes in estuarine systems either increase or decrease vulnerability to OA. Here, we quantified the relative impacts of OA (e.g., $\text{pH}_{\text{Base}} - \text{pH}_{\text{NOA}}$) and river basification (e.g., $\text{pH}_{\text{Base}} - \text{pH}_{\text{NBasi}}$) to long-term trends in surface pH and Ω_{Ar} along the main stem of Chesapeake Bay (Table 3). Contributions of processes other than OA and basification to pH trends (e.g., internal sources) were estimated as the remaining long-term trends after OA and river basification effects were removed (e.g., $\text{pH}_{\text{Base}} - \text{pH}_{\text{NOA}} - \text{pH}_{\text{NBasi}}$), assuming that all of the

Table 3
Contributions From Multiple Anthropogenic Forcing to the Long-Term Variability of pH and Ω_{Ar}

Location	Season	Total trend (30 years)	Ocean acidification	River basification	Biological and others	
pH	Upper	Spring	+0.150	-0.042 (18%)	+0.150 (64%)	+0.042 (18%)
		Summer	+0.033	-0.036 (20%)	+0.105 (60%)	-0.036 (20%)
	Mid	Spring	-0.129	-0.078 (43%)	+0.027 (14%)	-0.078 (43%)
		Summer	-0.141	-0.066 (38%)	+0.018 (10%)	-0.093 (52%)
	Lower	Spring	-0.177	-0.072 (36%)	+0.012 (6%)	-0.117 (58%)
		Summer	-0.114	-0.075 (57%)	+0.009 (7%)	-0.048 (36%)
Ω_{Ar}	Upper	Spring	+0.057	-0.021 (21%)	+0.045 (46%)	+0.033 (33%)
		Summer	+0.036	-0.036 (33%)	+0.063 (59%)	+0.009 (8%)
	Mid	Spring	-0.060	-0.150 (50%)	+0.120 (40%)	-0.030 (10%)
		Summer	-0.096	-0.192 (45%)	+0.165 (39%)	-0.069 (16%)
	Lower	Spring	-0.282	-0.192 (43%)	+0.084 (18%)	-0.174 (39%)
		Summer	-0.222	-0.180 (38%)	+0.126 (26%)	-0.168 (36%)

Note. Key contributions are highlighted in bold.

physical and biogeochemical process contributions were linearly additive. Surface water temperature in the three main stem regions increased 1.3–1.4°C in spring and 0.86–0.89°C in summer in the simulations of 1986–2015, consistent with recent reports (Ding & Elmore, 2015; Testa et al., 2018), and corresponding to an Ω_{Ar} increase of 0.004 in the upper bay and 0.01 in the middle and lower bay. This long-term increase in Ω_{Ar} associated with the surface water warming was removed from the overall trends to focus on the OA and basification effects. These temperature-adjusted results demonstrated that river basification was the dominant process in long-term upper-bay pH and Ω_{Ar} increases, accounting for the majority of total variability (Table 3, 62%/52% for pH/ Ω_{Ar}). Observed February–March chlorophyll-*a* has increased in the upper bay over this period (Figure S7; Testa et al., 2018), and if this increase was associated with elevated primary production, it would likely have contributed to an observed daytime pH increase (Waldbusser et al., 2011). In contrast, model simulations indicated that OA (47%/41% for pH/ Ω_{Ar}) was the dominant driver of significant pH and Ω_{Ar} declines in the lower bay. Enhanced buffer effects from river basification

in the lower bay were relatively small, particularly for pH (6.5%). The midbay pH was minimally affected by river basification compared to the OA (41%). Although the OA effect (48%) still played an important role in Ω_{Ar} declines in the midbay, river basification turned out to be another key mechanism in regulating the surface Ω_{Ar} (40%) in this region.

There were remaining trends in modeled pH and Ω_{Ar} after OA and river basification effects were removed that appear to be associated with modeled long-term changes in net ecosystem production (NEP = GPP - R). We estimated the potential impacts of NEP-induced variations in pH and Ω_{Ar} by calculating the DIC and TA changes (Δ DIC/ Δ TA) expected from modeled changes in NEP in each region under the Base scenario. Here, we ignored potential loss/gain of DIC associated with NEP-induced changes (e.g., subsequent air-sea exchange due to the surface water DIC change), to obtain estimated pH and Ω_{Ar} changes associated only with NEP (i.e., biological impacts). The results indicated that these biological impacts accounted for significant fraction of long-term variability in pH and Ω_{Ar} that was unexplained by OA and basification (Figure 10, Table 3). These estimated long-term pH declines due to lowered surface NEP were 124% (0.11 decline during 1986–2015) and 86% (0.074 decline) of the total variability not explained by OA or basification in the middle and lower bay. The biological process also explained 92% (0.145 decline) of the long-term Ω_{Ar} variability from all the unidentified processes in the lower bay. Thus, the

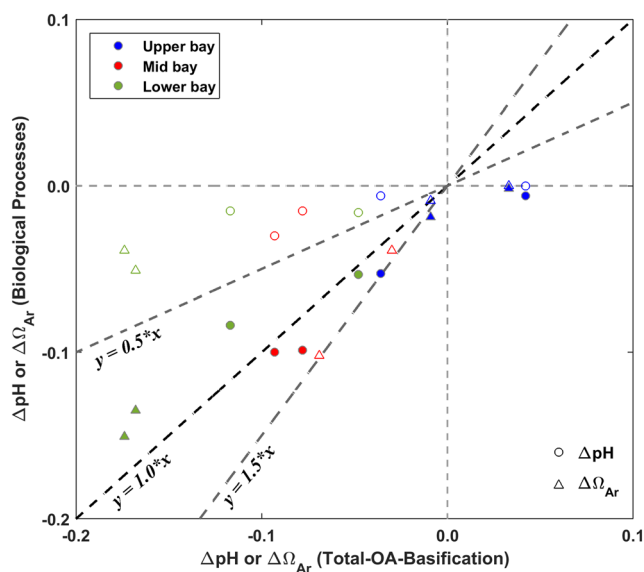


Figure 10. Relationship between modeled pH (circles) and Ω_{Ar} (triangles) changes in excess of that predicted from OA and basification (*x* axis) with pH and Ω_{Ar} changes associated with modeled trends in net ecosystem production (filled marker) and nutrient reduction (empty marker). Markers are colored by region (blue = upper; red = middle; green = lower) and both spring and summer periods are included for each region.

model simulations suggest that internal metabolic processes contribute to long-term pH and Ω_{Ar} changes at a comparable magnitude to OA and basification for lower-bay pH and Ω_{Ar} and midbay pH. These results are consistent with prior studies that have linked eutrophication to substantial diel, seasonal, and interannual variations in pH (Cai et al., 2017; Carstensen & Duarte, 2019; Duarte et al., 2013; Rheuban et al., 2019). It is worth mentioning that the model suggests a minor long-term reduction in bottom-water respiration (i.e., less DIC production) associated with reduced surface layer NEP, and this would have contributed an increase in pH (0.042/0.051 for middle and lower bay) and Ω_{Ar} (0.035/0.062) over the past 30 years.

The fact that a long-term trend in NEP was predicted by the model—and that this trend contributed to long-term trends in pH and Ω_{Ar} —reinforces the role of eutrophication in coastal acidification, but also demands further validation. The fact that trends in the model-simulated Chl *a* did not match those of the observations in the midbay during spring also requires explanation, especially considering that the long-term trend of modeled decreases in surface Chl-*a* was associated with a modeled decline in pH – both of which conflicted with available observations (Figures 7 and S7). Modeled declines in surface water NEP were associated with a slight decline in gross primary production (GPP) and a relatively constant respiration rate (R; Figure S8). Although the modeled decline in GPP is consistent with the reduction in nutrient loads, the changes in Chl *a* in simulations with the Susquehanna River nitrate load decline removed were relatively small (Figure S9). However, the boundary conditions used to force our 30-year simulation also include a decline in dissolved inorganic phosphorous load (~6% over 30 years) from the Susquehanna River and lower nitrate (~40%) and phosphorus (~16%) in the Potomac River, indicating additional nutrient reductions in the model that would contribute to lower NEP. Light attenuation (K_d) decreased in the model over 1986–2015, consistent with recent analyses of long-term observations (Harding et al., 2015), which presumably would have allowed for elevated GPP, opposite to what was observed. However, the decline in GPP with constant R over time led to lower net primary production (e.g., lower P/R ratio), leading to less Chl *a*. This pattern of lower P/R over time is, however, consistent with expectations of lower P/R ratios with warming (which occurred during the simulation) arising from the relatively higher sensitivity of R to temperature relative to photosynthesis (Yvon-Durocher et al., 2012). There are no long-term data for rates of GPP and R in the main stem over the full extent of the 1986–2015 period to validate this finding.

3.4. Model Limitations and Future Work

Model simulations presented here suggest long-term changes in carbonate chemistry associated with alterations of riverine, oceanic, and atmospheric forcing. A potential limitation of these simulations is the model's ability to reproduce historic pH patterns. Although the model-generated trends in pH matched observed trends in all but one of the regions and seasons analyzed (Figure 7), comparisons of observed and model-predicted pH revealed a relatively high RMSE (Figure 3). These mismatches can result from multiple sources of error in both the model and observations. First, it is not straightforward to correctly match observations made at a specific time and place to instances of time and space in a kilometer-scale model grid. In this analysis, we analyzed daily averaged model output and compared it to snapshot observations that are taken at one point in time, typically between morning and early afternoon. Because we know that pH can vary by 0.2–0.5 over the course of a day in the open main stem bay (Shen et al., 2019) and by even larger ranges in other locations, error in the comparison originates in part by selecting the exact model timeframe in which to compare to any given observation in time. A second source of error originates from the computation of modeled pH itself, which is calculated from modeled DIC and TA. Any errors associated with equilibrium constants or organic alkalinity would transfer to the model prediction of pH and using observational data collected in 2016 for pH, DIC, and TA, we note that directly measured pH and pH calculated using CO2SYS have an absolute mean error of 0.057–0.077, reflecting 27–37% of the magnitude of the RMSE we report (see Table S2). A third source of error lies in the monitoring program measurement of pH based upon glass potentiometric electrodes. There are many problems associated with this type of measurement in estuarine waters where differences in the ionic strength of calibration and measurement solutions can lead to drift and error in pH measurements (as reasoned in Waldbusser et al., 2011), or even where sensor responsiveness to rapidly changing pH over depth may not be fast enough given the speed of a vertical cast. These monitoring data are the best source of information we have to validate the model, and comparisons we made between measured pH with sensor pH (see Figure S10) were highly correlated with a slope close to 1 (slope = 0.95, $r^2 = 0.99$), but the absolute mean error was 0.12, indicating error that is ~50% of the

model-observation RMSE. Clearly, the biogeochemical and hydrodynamic processes in the model also impart error to the pH prediction, and further model performance could be improved by incorporating additional processes (e.g., SAV, improved calcification-dissolution dynamics, bivalve calcification) that have yet not been thoroughly identified and quantified to the carbonate system in estuarine environments as discussed in the following paragraph.

There has been a large resurgence in submerged aquatic vegetation (SAV) cover over the past several decades associated with the efforts to mitigate nutrient inputs and restore habitats across the bay-wide ecosystem (Lefcheck et al., 2018). Recently expanded SAV communities now cover up to 70% of the broad, tidal freshwater region at the mouth of Susquehanna River (in the very upper bay; Gurbisz & Kemp, 2014) and occupy several other low salinity regions of Chesapeake Bay (Orth et al., 2017). The metabolism of SAV increases the long-term offset of pH and Ω_{Ar} decrease due to OA (Pacella et al., 2018), and this might explain why the model predicted smaller long-term increases in the upper bay compared to the field observations (Figure 7) as benthic SAV was not considered in our model. The underestimation was especially clear during summer when observed SAV cover and density in this region peaks seasonally (Gurbisz et al., 2017). The Chesapeake Bay hosted massive precolonial oyster reefs, which historically removed about half of the total riverine alkalinity input, however, the alkalinity uptake by the oyster reefs had decreased by 100 fold by 1998 (Waldbusser et al., 2013). Shell dynamics could be important to the bay-wide carbonate chemistry given the large amount of active and buried shell material. Model simulations predicted a shoaling and seaward aragonite saturation horizon over the past 30 years, and future OA due to continuous anthropogenic CO₂ emissions could possibly lead to a more widespread dissolution-favorable environment ($\Omega_{Ar} < 1.0$, even in the lower bay), which could lead to elevated dissolution of carbonate minerals and if decoupled in space from precipitation environments, could potentially buffer against pH declines. Therefore, the incorporation of the SAV and shell dynamics modules to the existing hydrodynamic-biogeochemical model might better represent the interactions of multiple processes to estuarine carbonate chemistry, further strengthening the ability of process-based models for disentangling variable mechanisms.

Several recent efforts have illustrated either observed or projected enhancements of acidification across diverse coastal systems (Cai et al., 2011; Hauri et al., 2013; Rheuban et al., 2019), and similar trends toward acidification are evident in Chesapeake Bay, particularly the lower bay region. Given the important role of atmospheric and coastal ocean acidification in contributing to these trends in Chesapeake Bay, we have reason to suspect that acidification will continue. However, the duration, intensity, and spatial extent of unfavorable pH and saturation state conditions is difficult to predict, given the complex biogeochemical processes and direct impacts due to regional human activities and watershed management. Sensitivity scenarios in response to future atmospheric CO₂ indicated a further 0.075 pH reduction in the mainstem through direct CO₂ invasion associated with increased pCO_2 (~500 ppm) in the mid-21st century (Shen et al., 2019). However, estuarine ecosystem metabolism (e.g., photosynthesis, respiration) could be significantly altered via global warming and riverine nutrient delivery (Carstensen & Duarte, 2019; Pilcher et al., 2019) and future sea-level rise can influence biogeochemistry through the changes in saltwater intrusion, water temperature, and circulation. This high-resolution model, if driven by proper earth system projections and adapted to regional ecosystem management plans, would enable us to explore the future variability of carbonate system and anthropogenic impacts in Chesapeake Bay and other estuarine environments.

3.5. Management Implications of Estuarine Eutrophication and Acidification

Regional management actions to reverse eutrophication have been promoted since the 1980s to mitigate against estuarine hypoxia (low DO), reduced water clarity, and harmful algal blooms. However, observations suggest that nutrient loading reductions over the past several decades have only had a modest impact on Chl *a* along the main stem, with seasonal and regional-specific changes (Testa et al., 2018). Climatic variations also exert a strong influence on phytoplankton biomass and composition through alterations in river discharge and nutrient loading (Harding et al., 2015). Clearly, estuarine ecosystems do not simply follow linear trajectories and return directly to historic condition with decreased nutrient loading (Duarte et al., 2009; Harding et al., 2016), especially where loading reductions are modest. The total nitrogen and NO₂ + NO₃ inputs from the major tributaries have been reduced by ~17% and 14%, respectively, over the last three decades. Results of a model scenario without this nitrogen loading reduction indicated that the long-term

nutrient reductions had negligible impacts on the upper bay and contributed a small degree of euphotic layer Chl *a* reduction in the middle (~3.9%) and lower (~4.4%) bay (Figure S9), revealing nonlinear and diverse controls (i.e., nutrient, light, stratification, river discharge, etc.) on bay-wide phytoplankton biomass. The lowered primary production associated with reduced nutrient inputs corresponded to almost 25% of the total surface water pH/ Ω_{Ar} decline that we associated with unidentified biological processes (Figure 10): however, the midbay pH decline for bottom waters over the long-term period was slightly relieved during the summer period, with an overall increase of 0.03 compared to the Base scenario (Figure S11) consistent with observations of slightly elevated oxygen concentrations in this region in recent decades (Testa et al., 2018; Zhang et al., 2018). The Chl *a* reduction (as well as the pH/ Ω_{Ar} decline) associated with the nitrogen reduction could be underestimated by the model given that inputs from wastewater treatment plants (WWTPs) and atmospheric deposition were not considered. Steep reductions in nitrogen loading from WWTPs were achieved since 1985 due to facility upgrades and improved operational efficiency. The total nitrogen reduction from WWTPs in the Baltimore-Washington metropolitan area reached up to 80% (~11.86 Gg N/yr), which is slightly larger than the Susquehanna River reduction (~10.9 Gg N/yr), but these facilities discharge well upstream of the Chesapeake Bay main stem and their influence may be limited (Boynton et al., 1995) or seasonally dependent (Pennino et al., 2016). The bay-wide atmospheric DIN deposition reduction was estimated as 3.6 Gg N/yr, representing a ~24% reduction in that source, which is otherwise small compared to Susquehanna River inputs. While continuous but more aggressive nutrient reduction management is required for ecosystem restoration (e.g., to achieve bottom-water DO >1 mg L⁻¹, Harding et al., 2015), estuarine acidification poses a dilemma for regional eutrophication management because desired reductions of surface primary production could lead to further declines of surface water pH/ Ω_{Ar} , particularly in the middle and lower bay. The current average pH conditions in many oyster grounds are not suitable for shell preservation (Waldbusser et al., 2011), and continuing anthropogenic CO₂ emissions as well as watershed nutrient management could further lower pH/ Ω_{Ar} in shallow sites of middle and lower bay, therefore limiting calcification of shell-forming species and placing potential threats to bay-wide oyster restoration.

4. Conclusions

In this study, we investigated the anthropogenic impacts on pH and Ω_{Ar} over a long-term period (1986–2015) in Chesapeake Bay using a coupled hydrodynamic-biogeochemical model. Simulation results revealed a general pattern that pH and Ω_{Ar} increased with salinity and decreased with depth. Modeled long-term trends in carbonate chemistry under multiple anthropogenic stressors displayed spatial variations in both the magnitude and direction. The pH and Ω_{Ar} were more dynamic in the midbay region and there was a long-term increase in the annual duration of acidified bottom waters (pH < 7.5, ~2 days/yr) as well as a shallowing of the saturation horizon (~0.1 m/yr). The model predicted an increasing trend of surface-water pH and Ω_{Ar} in the upper bay, but an overall decreasing trend in the lower bay, consistent with observations. Scenario results demonstrated that the increasing trend in the upper bay was associated with increased alkalization of the Susquehanna River. Significant long-term pH and Ω_{Ar} declines in the lower bay were driven by nearly equal contributions from ocean acidification and lowered net ecosystem production. The midbay pH variability was primarily influenced by OA and biological process, while river basification along with OA played a key role in regulating the long-term Ω_{Ar} variability. This quantification of the spatially dependent contributions of eutrophication and long-term changes in freshwater and oceanic endmembers on estuarine acidification is instructive for natural resource management and ecosystem restoration in Chesapeake Bay and other similar coastal systems.

Data Availability Statement

Research data could be accessed on figshare at https://figshare.com/articles/RCA_Codes_and_boundary_forcing/12298862.

References

- Bakker, D., Pfeil, B., Landa, C. S., Metzl, N., O'Brien, K. M., Olsen, A., et al. (2016). A multi-decade record of high-quality FCO₂ data in version 3 of the Surface Ocean CO₂ Atlas (SOCAT). *Earth System Science Data*, 8(2), 383–413. <https://doi.org/10.5194/essd-8-383-2016>
- Bauer, J., Cai, W., Raymond, P. A., Bianchi, T. S., Hopkinson, C. S., & Regnier, P. A. (2013). The changing carbon cycle of the coastal ocean. *Nature*, 504(7478), 61–70. <https://doi.org/10.1038/nature12857>

Acknowledgments

This study was funded by the United States National Oceanic and Atmospheric Administration Ocean Acidification Program (NOAA-OAP; Awards NA15NOS4780184 and NA18NOS4780179). We also thank the US EPA Chesapeake Bay Program, Maryland Department of Natural Resources, Virginia Department of Environmental Quality, and United States Geological Survey for water monitoring data utilized in this study. This is UMCES contribution number 5863 and Ref. No. [UMCES] CBL 2020-132.

- Borges, A. V., & Gypens, N. (2010). Carbonate chemistry in the coastal zone responds more strongly to eutrophication than to ocean acidification. *Limnology and Oceanography*, *55*(1), 346–353. <https://doi.org/10.4319/lo.2010.55.1.0346>
- Boynton, W. R., Garber, J. H., Summers, R., & Kemp, W. M. (1995). Inputs, transformations, and transport of nitrogen and phosphorus in Chesapeake Bay and selected tributaries. *Estuaries*, *18*(1), 285–314. <https://doi.org/10.2307/1352640>
- Brady, D. C., Testa, J. M., Di Toro, D. M., Boynton, W. R., & Kemp, W. M. (2013). Sediment flux modeling: Calibration and application for coastal systems. *Estuarine, Coastal and Shelf Science*, *117*, 107–124. <https://doi.org/10.1016/j.ecss.2012.11.003>
- Brodeur, J., Chen, B., Su, J., Xu, Y.-Y., Hussain, N., Scaboo, K. M., et al. (2019). Chesapeake Bay inorganic carbon: Spatial distribution and seasonal variability. *Frontiers in Marine Science*, *6*, 99. <https://doi.org/10.3389/fmars.2019.00099>
- Cai, W., Hu, X., Huang, W., Murrell, M. C., Lehrter, J. C., Lohrenz, S. E., et al. (2011). Acidification of subsurface coastal waters enhanced by eutrophication. *Nature Geoscience*, *4*(11), 766–770. <https://doi.org/10.1038/ngeo1297>
- Cai, W., Huang, W., Luther, G. W., Pierrot, D., Li, M., Testa, J. M., et al. (2017). Redox reactions and weak buffering capacity lead to acidification in the Chesapeake Bay. *Nature Communications*, *8*, 369. <https://doi.org/10.1038/s41467-017-00417-7>
- Cai, W., & Wang, Y. (1998). The chemistry, fluxes, and sources of carbon dioxide in the estuarine waters of the Satilla and Altamaha Rivers, Georgia. *Limnology and Oceanography*, *43*(4), 657–668. <https://doi.org/10.4319/lo.1998.43.4.0657>
- Carstensen, J., Chierici, M., Gustafsson, B. G., & Gustafsson, E. (2018). Long-term and seasonal trends in estuarine and coastal carbonate systems. *Global Biogeochemical Cycles*, *32*, 497–513. <https://doi.org/10.1002/2017GB005781>
- Carstensen, J., & Duarte, C. M. (2019). Drivers of pH variability in coastal ecosystems. *Environmental Science & Technology*, *53*(8), 4020–4029. <https://doi.org/10.1021/acs.est.8b03655>
- Crosswell, J. G., Anderson, I. C., Stanhope, J. W., Van Dam, B., Brush, M. J., Ensign, S., et al. (2017). Carbon budget of a shallow, lagoonal estuary: Transformations and source-sink dynamics along the river-estuary-ocean continuum. *Limnology and Oceanography*, *62*(S1), S29–S45. <https://doi.org/10.1002/lno.10631>
- Dickson, A. G., Wesolowski, D. J., Palmer, D. A., & Mesmer, R. E. (1990). Dissociation constant of bisulfate ion in aqueous sodium chloride solutions to 250°C. *The Journal of Physical Chemistry*, *94*(20), 7978–7985. <https://doi.org/10.1021/j100383a042>
- Ding, H., & Elmore, A. J. (2015). Spatio-temporal patterns in water surface temperature from Landsat time series data in the Chesapeake Bay, USA. *Remote Sensing of Environment*, *168*, 335–348. <https://doi.org/10.1016/j.rse.2015.07.009>
- Doney, S. C. (2010). The growing human footprint on coastal and open ocean biogeochemistry. *Science*, *328*(5985), 1512–1516. <https://doi.org/10.1126/science.1185198>
- Duarte, C. M., Conley, D. J., Carstensen, J., & Sanchez-Camacho, M. (2009). Return to Neverland: Shifting baselines affect eutrophication restoration targets. *Estuaries and Coasts*, *32*(1), 29–36. <https://doi.org/10.1007/s12237-008-9111-2>
- Duarte, C. M., Hendriks, I. E., Moore, T. S., Olsen, Y. S., Steckbauer, A., Ramajo, L., et al. (2013). Is ocean acidification an open-ocean syndrome? Understanding anthropogenic impacts on seawater pH. *Estuaries and Coasts*, *36*(2), 221–236. <https://doi.org/10.1007/s12237-013-9594-3>
- Feely, R. A., Alin, S. R., Newton, J. A., Sabine, C. L., Warner, M., Devol, A. H., et al. (2010). The combined effects of ocean acidification, mixing, and respiration on pH and carbonate saturation in an urbanized estuary. *Estuary, Coastal and Shelf Science*, *88*(4), 442–449. <https://doi.org/10.1016/j.ecss.2010.05.004>
- Feely, R. A., Okazaki, R. R., Cai, W. J., Bednaršek, N., Alin, S. R., Byrne, R. H., & Fassbender, A. (2018). The combined effects of acidification and hypoxia on pH and aragonite saturation in the coastal waters of California current ecosystem and the northern Gulf of Mexico. *Continental Shelf Research*, *152*, 50–60. <https://doi.org/10.1016/j.csr.2017.11.002>
- Feely, R. A., Sabine, C. L., Lee, K., Berelson, W., Kleyvas, J., Fabry, V. J., & Millero, F. J. (2004). Impact of anthropogenic CO₂ on the CaCO₃ system in the oceans. *Science*, *305*(5682), 326–366.
- Gurbisz, C., & Kemp, W. M. (2014). Unexpected resurgence of a large submersed plant bed in Chesapeake Bay: Analysis of time series data. *Limnology and Oceanography*, *59*(2), 482–494. <https://doi.org/10.4319/lo.2014.59.2.0482>
- Gurbisz, C., Kemp, W. M., Cornwell, J. C., Sanford, L. P., Owens, M. S., & Hinkle, D. C. (2017). Interactive effects of physical and biogeochemical feedback processes in a large submersed plant bed. *Estuaries and Coasts*, *40*(6), 1626–1641. <https://doi.org/10.1007/s12237-017-0249-7>
- Hagens, M., Slomp, C. P., Meysman, F. J. R., Seitaj, D., Harlay, J., Borges, A. V., & Middelburg, J. J. (2015). Biogeochemical processes and buffering capacity concurrently affect acidification in a seasonally hypoxic coastal marine basin. *Journal of Geophysical Research: Biogeosciences*, *12*, 1561–1583. <https://doi.org/10.5194/bg-12-1561-2015>
- Hagy, J. D., Boynton, W. R., Keefe, C. W., & Wood, K. V. (2004). Hypoxia in Chesapeake Bay, 1950–2001: Long term change in relation to nutrient loading and river flow. *Estuaries*, *27*(4), 634–658. <https://doi.org/10.1007/BF02907650>
- Harding, L. W., Gallegos, C. L., Perry, E. S., Miller, W. D., Adolf, J. E., Mallonee, M. E., & Paerl, H. W. (2015). Long-term trends of nutrients and phytoplankton in Chesapeake Bay. *Estuaries and Coasts*, *39*(3), 664–681. <https://doi.org/10.1007/s12237-015-0023-7>
- Harding, L. W., Mallonee, M. E., Perry, E. S., Miller, W. D., Adolf, J. E., Gallegos, C. L., & Paerl, H. W. (2016). Variable climatic conditions dominate recent phytoplankton dynamics in Chesapeake Bay. *Scientific Reports*, *6*, 23773. <https://doi.org/10.1038/srep23773>
- Hauri, C., Gruber, N., Vogt, M., Doney, S. C., Feely, R. A., Lachkar, Z., et al. (2013). Spatiotemporal variability and long-term trends of ocean acidification in the California currents system. *Journal of Geophysical Research: Biogeosciences*, *10*, 193–216. <https://doi.org/10.5194/bg-10-193-2013>
- Herrmann, M., Najjar, R. G., Kemp, W. M., Alexander, R. B., Boyer, E. W., Cai, W. J., et al. (2015). Net ecosystem production and organic carbon balance of U.S. East Coast estuaries: A synthesis approach. *Global Biogeochemical Cycles*, *29*, 96–111. <https://doi.org/10.1002/2013GB004736>
- Kaushal, S. S., Likens, G. E., Pace, M. L., Utz, R. M., Haq, S., Gorman, J., & Grese, M. (2018). Freshwater salinization syndrome on continental scale. *Proceedings of the National Academy of Sciences of the United States of America*, *115*(4), E574–E583. <https://doi.org/10.1073/pnas.1711234115>
- Kaushal, S. S., Likens, G. E., Utz, R. M., Pace, M. L., Grese, M., & Yepsen, M. (2013). Increased river Alkalinization in the eastern U.S. *Environmental Science & Technology*, *47*, 10,302–10,311. <https://doi.org/10.1021/es401046s>
- Kemp, W. M., Smith, E. M., Marvin-DiPasquale, M., & Boynton, W. R. (1997). Organic carbon balance and net ecosystem metabolism in Chesapeake Bay. *Marine Ecology Progress Series*, *150*, 229–248. <https://doi.org/10.3354/meps150229>
- Laurent, A., Fennel, K., Cai, W.-J., Huang, W.-J., Barbero, L., & Wanninkhof, R. (2017). Eutrophication-induced acidification of coastal waters in the northern Gulf of Mexico: Insights into origin and processes from a coupled physical-biogeochemical model. *Geophysical Research Letters*, *44*, 946–956. <https://doi.org/10.1002/2016GL071881>
- Laurent, A., Fennel, K., Ko, D. S., & Lehrter, J. (2018). Climate change projected to exacerbate impacts of coastal eutrophication in the northern Gulf of Mexico. *Journal of Geophysical Research: Oceans*, *123*, 3408–3426. <https://doi.org/10.1002/2017JC013583>

- Lefcheck, J., Orth, R. J., Dennison, W. C., Wilcox, D. J., Murphy, R. R., Keisman, J., et al. (2018). Long-term nutrient reductions lead to the unprecedented recovery of a temperate coastal region. *Proceedings of the National Academy of Sciences of the United States of America*, *115*(14), 3658–3662. <https://doi.org/10.1073/pnas.1715798115>
- Lewis, E. R., & Wallace, D. W. R. (1998). CO2SYS-Program developed for CO₂ system calculations. Carbon Dioxide Inf. Anal. Centre. <https://doi.org/10.2172/639712>
- Li, M., Lee, Y. J., Testa, J. M., Li, Y., Ni, W., Kemp, W. M., & Di Toro, D. M. (2016). What drives interannual variability of hypoxia in Chesapeake Bay: Climate forcing versus nutrient loading? *Geophysical Research Letters*, *43*, 2127–2134. <https://doi.org/10.1002/2015GL067334>
- Li, M., Zhong, L., & Boicourt, W. (2005). Simulations of Chesapeake Bay estuary: Sensitivity to turbulence mixing parameterizations and comparison with observations. *Journal of Geophysical Research*, *110*, C12004. <https://doi.org/10.1029/2004JC002585>
- Long, W. C., Swiney, K. M., & Foy, R. J. (2016). Effects of high pCO₂ on Tanner crab reproduction and early life history, Part II: carryover effects on larvae from oogenesis and embryogenesis are stronger than direct effects. *ICES Journal of Marine Science*, *73*, 836–848. <https://doi.org/10.1093/icesjms/fsv251>
- Marvin-DiPasquale, M., & Capone, D. (1998). Benthic sulfate reduction along the Chesapeake Bay central channel. I. Spatial trends and controls. *Marine Ecology Progress Series*, *168*, 213–228. <https://doi.org/10.3354/meps168213>
- Mucci, A., Starr, M., Gilbert, D., & Sundby, B. (2011). Acidification of lower St. Lawrence estuary bottom waters. *Atmosphere-Ocean*, *49*(3), 206–218. <https://doi.org/10.1080/07055900.2011.599265>
- Müller, J. D., Schneider, B., & Rehder, G. (2016). Long-term alkalinity trends in the Baltic Sea and their implications for CO₂-induced acidification. *Limnology and Oceanography*, *61*(6), 1984–2002. <https://doi.org/10.1002/lno.10349>
- Murphy, R. R., Kemp, W. M., & Ball, W. (2011). Long-term trends in Chesapeake Bay seasonal hypoxia, stratification, and nutrient loading. *Estuaries and Coasts*, *34*(6), 1293–1309. <https://doi.org/10.1007/s12237-011-9413-7>
- Orth, R., Dennison, W. C., Lefcheck, J. S., Gurbisz, C., Hannam, M., Keisman, J., et al. (2017). Submersed aquatic vegetation in Chesapeake Bay: Sentinel species in a changing world. *BioScience*, *67*, 689–712. <https://doi.org/10.1093/biosci/bix058>
- Pacella, S. R., Brown, C. A., Waldbusser, G. G., Labiosa, R. G., & Hales, B. (2018). Seagrass habitat metabolism increases short-term extremes and long-term offset of CO₂ under future ocean acidification. *Proceedings of the National Academy of Sciences*, *201703445*, 115(15), 3870–3875. <https://doi.org/10.1073/pnas.1703445115>
- Pennino, M. J., Kaushal, S. S., Murthy, S. N., Blomquist, J. D., Cornwell, J. C., & Harris, L. A. (2016). Sources and transformations of anthropogenic nitrogen along an urban river-estuarine continuum. *Journal of Geophysical Research: Biogeosciences*, *13*, 6211–6228. <https://doi.org/10.5194/bg-13-6211-2016>
- Pilcher, D. J., Naiman, D. M., Cross, J. N., Hermann, A. J., Siedlecki, S. A., Gibson, G. A., & Mathis, J. T. (2019). Modeled effect of coastal biogeochemical processes, climate variability, and ocean acidification on aragonite saturation state in the Bering Sea. *Frontiers in Marine Science*, *5*, 508. <https://doi.org/10.3389/fmars.2018.00508>
- Raymond, P. A., Oh, N. H., Turner, R. E., & Broussard, W. (2008). Anthropogenically enhanced fluxes of water and carbon from the Mississippi River. *Nature*, *451*(7177), 449–452. <https://doi.org/10.1038/nature06505>
- Regnier, P., Friedlingstein, P., Ciais, P., Mackenzie, F. T., Gruber, N., Janssens, I. A., et al. (2013). Anthropogenic perturbation of the carbon fluxes from land to ocean. *Nature Geoscience*, *6*(8), 597–607. <https://doi.org/10.1038/ngeo1830>
- Rheuban, J. E., Doney, S. C., McCorkle, D. C., & Jakuba, W. (2019). Quantifying the effects of nutrient enrichment and freshwater mixing on coastal ocean acidification. *Journal of Geophysical Research: Oceans*, *124*, 9085–9100. <https://doi.org/10.1029/2019JC015556>
- Riley, J. P., & Tongudai, M. (1967). The major cation/chlorinity ratios in sea water. *Chemical Geology*, *2*, 263–269. [https://doi.org/10.1016/0009-2541\(67\)90026-5](https://doi.org/10.1016/0009-2541(67)90026-5)
- Shen, C., Testa, J. M., Li, M., Cai, W. J., Waldbusser, G. G., Ni, W., et al. (2019). Controls on carbonate system dynamics in a coastal plain estuary: A modelling study. *Journal of Geophysical Research: Biogeosciences*, *124*, 61–78. <https://doi.org/10.1029/2018JG004802>
- Siedlecki, S. A., Pilcher, D. J., Hermann, A. J., Coyle, K., & Mathis, J. (2017). The importance of freshwater to spatial variability of aragonite saturation state in the Gulf of Alaska. *Journal of Geophysical Research: Oceans*, *122*, 8482–8502. <https://doi.org/10.1002/2017JC012791>
- Smith, E. M., & Kemp, W. M. (1995). Seasonal and regional variations in plankton community production and respiration for Chesapeake Bay. *Marine Ecology Progress Series*, *116*, 217–231. <https://doi.org/10.3354/meps116217>
- Sunda, W. G., & Cai, W.-J. (2012). Eutrophication induced CO₂ acidification of subsurface coastal waters: Interactive effects of temperature, salinity and atmosphere pCO₂. *Environmental Science & Technology*, *46*(19), 10,651–10,659. <https://doi.org/10.1021/es300626f>
- Testa, J. M., Brady, D. C., Di Toro, D. M., Boynton, W. R., Cornwell, J. C., & Kemp, W. M. (2013). Sediment flux modeling: Nitrogen, phosphorus and silica cycles. *Estuarine, Coastal and Shelf Science*, *131*, 245–263. <https://doi.org/10.1016/j.ecss.2013.06.014>
- Testa, J. M., & Kemp, W. M. (2012). Hypoxia-induced shifts in nitrogen and phosphorus cycling in Chesapeake Bay. *Limnology and Oceanography*, *57*(3), 835–850. <https://doi.org/10.4319/lno.2012.57.3.0835>
- Testa, J. M., Li, Y., Lee, Y., Li, M., Brady, D. M., Di Toro, D., et al. (2014). Quantifying the effects of nutrient loading on dissolved O₂ cycling and hypoxia in Chesapeake Bay using a coupled hydrodynamic-biogeochemical model. *Journal of Marine Systems*, *139*, 139–158. <https://doi.org/10.1016/j.jmarsys.2014.05.018>
- Testa, J. M., Murphy, R. R., Brady, D. C., & Kemp, W. M. (2018). Nutrient- and climate-induced shifts in the phenology of linked biogeochemical cycles in a temperate estuary. *Frontiers in Marine Science*, *5*. <https://doi.org/10.3389/fmars.2018.00114>
- Van Dam, B. R., & Wang, H. (2019). Decadal-scale acidification trends in adjacent North Carolina estuaries: Competing role of anthropogenic CO₂ and riverine alkalinity loads. *Frontiers in Marine Science*, *6*, 136. <https://doi.org/10.3389/fmars.2019.00136>
- Waldbusser, G. G., Hales, B., Langdon, C. J., Haley, B. A., Schrader, P., Brunner, E. L., et al. (2015). Experimental evidence for saturation state impacts on early larval bivalves. *Nature Climate Change*, *5*(3), 273–280. <https://doi.org/10.1038/NCLIMATE2479>
- Waldbusser, G. G., Powell, E. N., & Mann, R. (2013). Ecosystem effects of shell aggregations and cycling in coastal waters: Example of Chesapeake Bay oyster reefs. *Ecology*, *94*(4), 895–903. <https://doi.org/10.1890/12-1179.1>
- Waldbusser, G. G., & Salisbury, J. E. (2014). Ocean acidification in the coastal zone from an organism's perspective: Multiple system parameters, frequency domains, and habitats. *Annual Review of Marine Science*, *6*(1), 221–247. <https://doi.org/10.1146/annurev-marine-121211-172238>
- Waldbusser, G. G., Voigt, E. P., Bergschneider, H., Green, M. A., & Newell, R. I. E. (2011). Biocalcification in the eastern oyster (*Crassostrea virginica*) in relation to long-term trends in Chesapeake Bay pH. *Estuaries and Coasts*, *34*(2), 221–231. <https://doi.org/10.1007/s12237-010-9307-0>
- Wallace, R. B., Baumann, H., Gear, J. S., Aller, R. C., & Golber, C. J. (2014). Coastal ocean acidification: The other eutrophication problem. *Estuarine, Coastal and Shelf Science*, *148*, 1–13. <https://doi.org/10.1016/j.ecss.2014.05.027>

- Xu, Y., Cai, W.-J., Gao, Y., Wanninkhof, R., Salisbury, J., Chen, B., et al. (2017). Short-term variability of aragonite saturation state in the central mid-Atlantic bight. *Journal of Geophysical Research: Oceans*, *122*, 4274–4290. <https://doi.org/10.1002/2017JC012901>
- Yvon-Durocher, G., Caffrey, J. M., Cescatti, A., Dossena, M., del Giorgio, P., Gasol, J. M., et al. (2012). Reconciling the temperature dependence of respiration across timescales and ecosystem types. *Nature*, *487*(7408), 472–476. <https://doi.org/10.1038/nature11205>
- Zhang, Q., Brady, D. C., Boynton, W. R., & Ball, W. P. (2015). Long-term trends of nutrients and sediment from the nontidal Chesapeake watershed: An assessment of progress by river and season. *Journal of the American Water Resources Association*, *51*(6), 1534–1555. <https://doi.org/10.1111/1752-1688.12327>
- Zhang, Q., Tango, P. J., Murphy, R. R., Forsyth, M. K., Tian, R., Keisman, J., & Trentacoste, E. M. (2018). Chesapeake Bay dissolved oxygen criterion attainment deficit: Three decades of temporal and spatial patterns. *Frontiers in Marine Science*, *5*, 422. <https://doi.org/10.3389/fmars.2018.00422>
- Zhong, L., & Li, M. (2006). Tidal energy fluxes and dissipation in the Chesapeake Bay. *Continental Shelf Research*, *26*(6), 752–770. <https://doi.org/10.1016/j.csr.2006.02.006>